

Kinematics, dynamics, and control system of a new 5-degree-of-freedom hybrid robot manipulator

Advances in Mechanical Engineering
2016, Vol. 8(1) 1–19
© The Author(s) 2016
DOI: 10.1177/1687814016680309
aim.e.sagepub.com



Wanjin Guo¹, Rui Feng Li¹, Chuqing Cao^{2,3} and Yunfeng Gao¹

Abstract

Hybrid robotic application is a continuously developing field, as hybrid robot manipulators have demonstrated clearly to possess benefits of both serial structures and parallel mechanisms. In this article, the physical prototype and the specially designed control system for a new 5-degree-of-freedom hybrid robot manipulator are developed. The mechanical structure, kinematics, dynamics, and control system of this robot manipulator are presented. A newly appropriate set of closed-form solutions, which can avoid multiple solutions, is proposed to address the inverse kinematics problem of this robot manipulator. Additionally, simulations of the kinematics and dynamics of this robot manipulator and the tests for the repeatability and accuracy of both the position and path are first simulated with two numerical examples and then conducted on the physical prototype.

Keywords

Robotics, hybrid robot manipulator, kinematics, dynamics, control system

Date received: 23 August 2016; accepted: 30 October 2016

Academic Editor: Fakher Chaari

Introduction

More and more hybrid robotic systems are nowadays designed and developed with advanced technology in recent years.^{1–5} The superiority of the hybrid robot stems from the combined benefits of the large workspace provided by the serial mechanism and the high stiffness advantage offered by the parallel mechanism. Several 5-degree-of-freedom (DOF) hybrid robot manipulators were investigated and devoted to advanced applications in some fascinating fields.

Several studies were concentrated on 5-DOF hybrid robot manipulators for surface machining and fabrication applications. A 5-DOF hybrid mechanism, which includes a synthesized 2 translational DOFs and 1 rotational DOF (2T1R) parallel module, was developed.^{6–8} A 3-DOF parallel platform and a X-Y table were integrated into a 5-DOF hybrid mechanism.⁹ Another 5-DOF hybrid robot manipulator was proposed, which consists of a parallel mechanism (3T1R) and a

rotational table.¹⁰ Altuzarra et al.¹¹ designed a 5-DOF hybrid mechanism which includes a parallel manipulator (2T1R) with a rotational table. Several research works were presented for 5-DOF hybrid robot manipulators with redundantly actuated joint or passive joint. A 5-DOF hybrid mechanism including a 2-DOF redundant parallel manipulator was studied.¹² Another 5-DOF hybrid mechanism, consisting of a 3-DOF

¹State Key Laboratory of Robotics and System, Harbin Institute of Technology, Harbin, P.R. China

²School of Mechanical Engineering, Nanjing University of Science and Technology, Nanjing, P.R. China

³Wuhu HIT Robot Technology Research Institute Co., Ltd, Wuhu, P.R. China

Corresponding author:

Wanjin Guo, State Key Laboratory of Robotics and System, Harbin Institute of Technology, 92 West Dazhi Street, Nan Gang District, Harbin 150001, P.R. China.

Email: guowanjin0102@gmail.com



Creative Commons CC-BY: This article is distributed under the terms of the Creative Commons Attribution 3.0 License (<http://www.creativecommons.org/licenses/by/3.0/>) which permits any use, reproduction and distribution of the work without further permission provided the original work is attributed as specified on the SAGE and Open Access pages (<https://us.sagepub.com/en-us/nam/open-access-at-sage>).

parallel manipulator with actuation redundancy and a 2-DOF worktable, was investigated.^{13–15} Jiang et al.¹⁶ developed a 5-DOF hybrid-driven magnetic resonance-compatible robot for minimally invasive prostatic interventions. A 5-DOF surgical hybrid robot, which consists of a 3-DOF parallel module and a 2-DOF serial module, was designed.¹⁷ Several other 5-DOF hybrid robots were reported. A 5-DOF hybrid robot, which comprises a parallel mechanism (1T2R) and two gantries, was introduced.¹⁸ Two 5-DOF mechanisms, which are composed of a 3-DOF parallel mechanism connected in series with a 2-DOF wrist, were introduced.¹⁹ A 5-DOF hybrid robot, consisting of a 3-DOF kinematic mechanism and a 2-DOF parallel mechanism, was designed.²⁰ Another reconfigurable 5-DOF hybrid robot, which consists of a 2-DOF rotatable mechanism and a 3-DOF parallel mechanism, was proposed.²¹ These 5-DOF hybrid robot manipulators have several disadvantages. Some designs of robot manipulators are very complex, since an application of the inferior-mobility robot manipulator demands a translatable table^{6–8} or a rotatable one.^{9–11} Also, the problem of achieving motion control is harder for the hybrid mechanism^{12–15} with redundantly actuated joints than a non-redundantly actuated one. Likewise, the motion control of the robots^{16,17} with passive joints is more difficult than those without passive joints. Moreover, some 5-DOF hybrid robot manipulators^{19–21} are established to perform the tasks in a relatively small accessible workspace.

Several research works were presented for kinematic analysis, dynamic analysis, and control system of robot manipulators. A general approach was proposed for Jacobian analysis of serial-parallel manipulators based on the unified Jacobian model.²² A unifying framework was presented for the study of the statics and the instantaneous kinematics of robot manipulators based on the Grassmann–Cayley algebra.²³ Closed-form solutions to the forward and inverse kinematic problems and an approach to formulation of the basic kinematic equations for a hybrid manipulator were studied.²⁴ The inverse dynamic model was usually derived using recursive Newton–Euler algorithm (RNEA),²⁵ Lagrangian formulation,¹⁰ or Kane’s approach.²⁶ The design concepts and approaches to building software and hardware architecture of the robot manipulator control system were described in Krasilnikyants et al.²⁷ A fuzzy-neural-network inherited sliding-mode control system was presented for an n-link robot manipulator.²⁸ A control system with a decoupled and centralized control structure was designed for a heavy-duty industrial robot.²⁹

Principles for the efficient processing of complex surfaces can be extended to the representation of complex movements and actions, where the 5-DOF machine tool with hybrid architecture can properly fit in. It is well

known that the hybrid machine can combine the benefits of the serial and parallel mechanisms while avoiding the drawbacks of either. Thus, the hybrid structure is helpful to allow a flexible axis arrangement and enlarge a workspace on the premise of moderate complexity. For these motivations, the geometric configuration, the kinematics, and the reachable workspace of a new 5-DOF hybrid robot manipulator were proposed in our other article.³⁰ In this article, the developed physical prototype and the tests for the repeatability and accuracy of this new 5-DOF hybrid robot manipulator are presented. A newly appropriate set of closed-form solutions, which can avoid multiple solutions, is proposed to improve the already proposed set of closed-form solutions in our article³⁰ for this robot manipulator. The inverse kinematics and inverse dynamic problems of this robot manipulator are solved through this proposed algebraic method (to find closed-form solutions) and the RNEA (to derive inverse dynamic equations), respectively. Two numerical examples are presented to verify the kinematics and dynamics of this robot manipulator, respectively. Moreover, a control system is specially designed for this robot manipulator, with which two experiments are conducted on the physical prototype to test the repeatability and accuracy of both the path and position.

The rest of this article is organized as follows. The structure of the developed robot manipulator is described in section “Structure of the robot manipulator.” The forward and inverse kinematics of this manipulator are presented in section “Kinematics of the robot manipulator.” The inverse dynamic problem of this robot manipulator is solved in section “Dynamics of the robot manipulator.” The specially designed control system for this robot manipulator is described in section “Control system of the robot manipulator.” Numerical examples for verifying the kinematics modeling and dynamics modeling and the experiments for the repeatability and accuracy of both the position and path are shown in section “Numerical examples and experiments.” Finally, conclusions are drawn in section “Conclusion.”

Structure of the robot manipulator

The configuration and drive system of this developed 5-DOF hybrid robot manipulator are presented in this section. More details of other related structure analysis, advantages, and the overall performance descriptions of this hybrid robot manipulator are introduced in our article.³⁰

In order to obtain good dexterity in robot manipulation and also meet good performance requirements, a hybrid configuration is employed in the developed robot manipulator. The first 2 DOFs are realized by a

parallel mechanism provided sufficient structural stiffness, and its drive system is less complicated in practical implementation. The last 3 DOFs are realized by a cantilever-like mechanism. It provides this robot manipulator with an increased level of dexterity and enhanced motion control and help meet the requirement of the reachable workspace. Despite the trade-off being made on the rigidity of the manipulator's overall structure when using the cantilever-like mechanism, the ultimate goal of designing a robot manipulator structure with relatively high structural stiffness, good manipulation dexterity, and excellent motion capabilities can be realized by this hybrid design configuration.

The physical prototype and the structure of this developed 5-DOF robot manipulator are shown in Figure 1. This robot manipulator, consisting of a 3-DOF (3T) parallel module and a 2-DOF (2R) serial module, is a new 3T2R hybrid robot manipulator. Translational motion axes J_1 , J_2 , and J_3 are ball screws driven by motors M_1 , M_2 , and M_3 , respectively. Rotational motion axes J_4 and J_5 are driven by motors M_4 and M_5 , respectively. Axis J_6 is the end-effector that contains a high-speed motor spindle.

The primary feature of this designed robot manipulator is the good dexterity performance which benefits from the ingeniously mechanical arrangements, that is, the decoupling control adjustments of the orientation and position of the end-effector can be achieved when

the structure parameter e is equal to 0. The other main mechanical structure features are as follows: (a) a parallel-driven component consisting of two ball screw-based linear drives is designed to generate the translational movement of the robot manipulator in the horizontal plane, and this drive arrangement simplifies the configuration, strengthens transmission stiffness, and reduces cost; (b) a long straight rail component with gantry mechanism characteristic features is applied, which reduces the mass and gravity moments and transfers the majority of the gravity and overture moments from the robot manipulator to the base framework; and (c) three ball screw-based linear drives are used to provide a simplified transmission and significant cost savings and eliminate the need for relatively expensive reducer.

Compared with a general 6R serial robot, this novel robot manipulator offers the following particular advantages: (a) the decoupling control of the position and orientation of the end-effector; this allows the inverse kinematics to take advantage of particular geometric features of the robot manipulator in its unique solution, whereas a general 6R serial robot cannot exhibit this kind of superiority; (b) the parallel-driven component and the long straight rail component can reduce the separate drive requirements and transfer the majority of the mass and gravity moments from the robot manipulator to the base framework; in the case of a

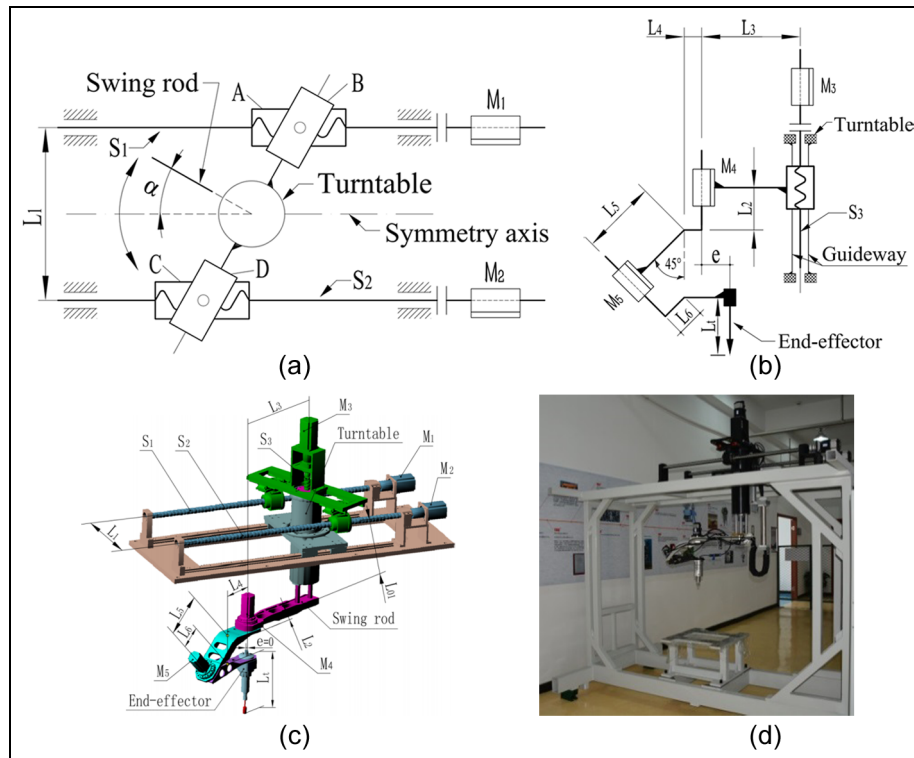


Figure 1. Robot manipulator: (a) top view, (b) front view, (c) 3D model, and (d) physical prototype.

general 6R serial robot, the waist joint is needed to support the heavy loads and overturn moments of the whole body; and (c) ball screw-based linear drives without the expensive rotary vector (RV) or harmonic drive can reduce significantly larger cost savings than a general 6R serial robot.

This developed robot manipulator is aimed at the deburring application of the aluminum alloy parts in the automobile industry, such as engine head. When a robot manipulator performs some operations on a surface, especially a complex surface, the capability of high manipulation dexterity and even the capability of five-face machining in one setup are required and are imperative. The burrs of the part which requires five-face deburring can be removed in one setup, since this developed robot manipulator has the capability to be serviced for five-face machining in one setup. The deburring application of parts with complex surfaces can benefit from the superiority of dexterity in orientation adjustment, positioning, and trajectory tracking control. Also, other machining applications in industrial settings, such as milling and drilling, can be achieved using different sets of machining tools.

Kinematics of the robot manipulator

In this section, the reference frames and the forward kinematics solution for this robot manipulator are presented based on the Denavit–Hartenberg method. In addition, a newly appropriate set of closed-form solutions (which can avoid multiple solutions) is proposed to improve the already proposed set of closed-form

solutions (which has the possibility of multiple solutions) in our article³⁰ for solving the inverse kinematics problem. Here, the concepts of the equivalent axis and the equivalent angle which are applied to verify the orientation validity of the forward kinematics solution can be referred to our article.³⁰

Forward kinematics

The Denavit–Hartenberg method³¹ is applied to model the kinematics of this robot manipulator. The reference frames for this robot manipulator are assigned as shown in Figure 2. The rotation angles of J_1, J_2, J_3, J_4 , and J_5 are expressed by $\varphi_1, \varphi_2, \varphi_3, \varphi_4$, and φ_5 , respectively. The strokes of the nut along S_1, S_2 , and S_3 are expressed by X_1, X_2 , and X_3 , respectively. The distance between J_6 and J_4 in the horizontal direction is denoted as e . The rotation angle of J_t and link 1 is denoted as α . L_i denotes the length of rod i . L_{01} represents the distance between origin O_2 and origin O_1 in the vertical direction when the nut is located at the top starting point along S_3 . The detailed structure parameters of this robot manipulator are listed in Table 1. These variables can be expressed by

$$\alpha = \arctan\left(\frac{(X_2 - X_1)}{L_1}\right) \quad (1)$$

$$X_1 = \frac{s_x \varphi_1}{2\pi} \quad (2)$$

$$X_2 = \frac{s_x \varphi_2}{2\pi} \quad (3)$$

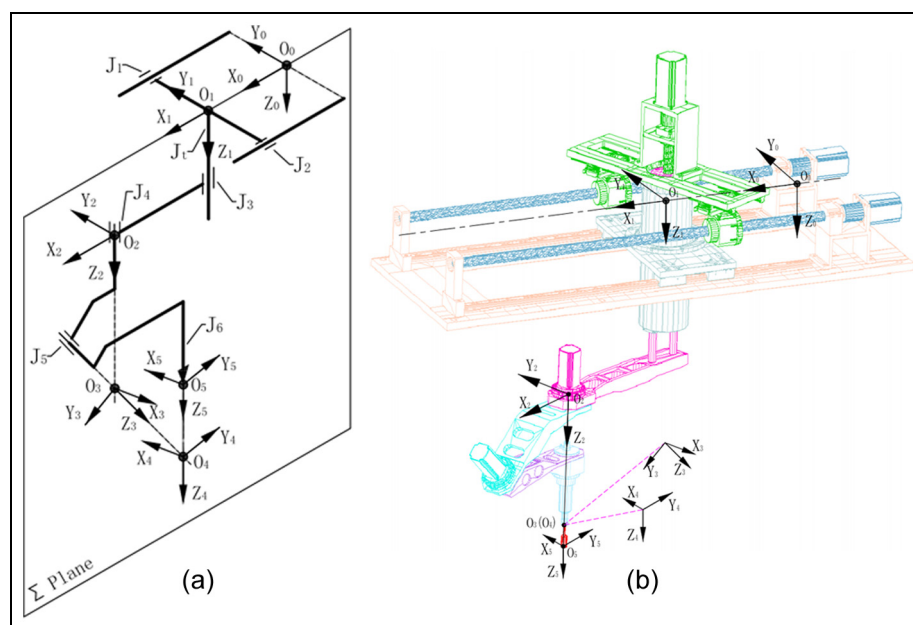


Figure 2. The assigned reference frame: (a) Denavit–Hartenberg reference frame and (b) the location of D–H reference frame.

Table 1. Robot manipulator structure parameters (mm).

L_1	L_2	L_3	L_4	L_5	L_6	e	L_t	L_{01}	s_x	s_z
420	50	450	160	210	95	0	285	465	10	10

Table 2. Geometry parameters of the robot manipulator.

Link i	θ_i	α_i	d_i	a_i
2	0	0	$X_3 + L_{01}$	L_3
3	$-\pi/2 + \varphi_4$	$\pi/4$	$L_2 + L_4 + \sqrt{2}L_5$	0
4	$\pi + \varphi_5$	$\pi/4$	$\sqrt{2}e$	0
5 (Tool)	0	0	L_p	0

$$X_3 = \frac{s_z \varphi_3}{2\pi} \quad (4)$$

where the constant s_x represents the pitch of S_1 and S_2 , the constant s_z represents the pitch of S_3 , and the available range of the rotation angle is $\alpha \in [-\pi/4, \pi/4]$ because of the mechanical constraints.

Link 1 is driven in parallel by M_1 and M_2 , as shown in Figures 1 and 2, and a coupled movement is generated (i.e. link 1 moves along axis X_1 , the axis of symmetry of screws S_1 and S_2 , and it also rotates with the turntable about J_t when the strokes of nuts connecting A and C along the screw are different). While link 1 rotates about Z_1 and J_t , its moving direction along axis X_1 is always parallel to X_0 . Based on this relationship, the spatial displacement of reference frame 1 to base reference frame 0, that is, 0T_1 , can be directly obtained as

$${}^0T_1 = \begin{bmatrix} \cos \alpha & -\sin \alpha & 0 & (X_1 + X_2)/2 \\ \sin \alpha & \cos \alpha & 0 & 0 \\ 0 & 0 & 1 & 0 \\ 0 & 0 & 0 & 1 \end{bmatrix} \quad (5)$$

where

$$\cos \alpha = \frac{L_1}{\sqrt{(X_2 - X_1)^2 + L_1^2}} \quad (6)$$

$$\sin \alpha = \frac{(X_2 - X_1)}{\sqrt{(X_2 - X_1)^2 + L_1^2}} \quad (7)$$

Let L_p be defined as the tool compensation, which is the value of the tool frame point O_5 in Z_4 axis given as

$$L_p = L_t - (L_4 + \sqrt{2}L_6 + e) \quad (8)$$

The geometric parameters of links 2, 3, 4, and 5 (tool) for this 5-DOF robot manipulator are listed in Table 2.

The homogeneous transformation matrix ${}^{i-1}T_i$ is conducted to represent reference frame i relative to frame $i-1$ according to the assigned reference frames and the geometry parameters; it is defined by

$${}^{i-1}T_i = \begin{bmatrix} \cos \theta_i & -\cos \alpha_i \cdot \sin \theta_i & \sin \alpha_i \cdot \sin \theta_i & a_i \cdot \cos \theta_i \\ \sin \theta_i & \cos \alpha_i \cdot \cos \theta_i & -\sin \alpha_i \cdot \cos \theta_i & a_i \cdot \sin \theta_i \\ 0 & \sin \alpha_i & \cos \alpha_i & d_i \\ 0 & 0 & 0 & 1 \end{bmatrix} \quad (9)$$

where $i = 2, \dots, 5, i \in N$.

The equivalent homogeneous transformation matrix 0T_5 , which relates the spatial displacement of the end-effector reference frame to the base reference frame, can be obtained by successive multiplications of these transformation matrices

$${}^0T_5 = {}^0T_1 {}^1T_2 {}^2T_3 {}^3T_4 {}^4T_5 = \begin{bmatrix} n_x & o_x & a_x & p_x \\ n_y & o_y & a_y & p_y \\ n_z & o_z & a_z & p_z \\ 0 & 0 & 0 & 1 \end{bmatrix} \quad (10)$$

where

$$\vec{p} = [p_x, p_y, p_z]^T \quad (11)$$

$$p_x = \frac{(X_1 + X_2)}{2} - e \cos(\alpha + \varphi_4) + L_3 \cos \alpha + L_p \left[\frac{\cos(\alpha + \varphi_4)(\cos \varphi_5 - 1)}{2} - \frac{\sin(\alpha + \varphi_4) \sin \varphi_5}{\sqrt{2}} \right] \quad (12)$$

$$p_y = L_3 \sin \alpha - e \sin(\alpha + \varphi_4) + L_p \left[\frac{\sin(\alpha + \varphi_4)(\cos \varphi_5 - 1)}{2} + \frac{\cos(\alpha + \varphi_4) \sin \varphi_5}{\sqrt{2}} \right] \quad (13)$$

$$p_z = L_2 + L_4 + \sqrt{2}L_5 + X_3 + L_{01} + e + L_p \frac{(1 + \cos \varphi_5)}{2} \quad (14)$$

$$\vec{a} = [a_x, a_y, a_z]^T \quad (15)$$

$$a_x = \frac{\cos(\alpha + \varphi_4)(\cos \varphi_5 - 1)}{2} - \frac{\sin(\alpha + \varphi_4)\sin \varphi_5}{\sqrt{2}} \quad (16)$$

$$a_y = \frac{\sin(\alpha + \varphi_4)(\cos \varphi_5 - 1)}{2} + \frac{\cos(\alpha + \varphi_4)\sin \varphi_5}{\sqrt{2}} \quad (17)$$

$$a_z = \frac{(1 + \cos \varphi_5)}{2} \quad (18)$$

$$\vec{o} = [o_x, o_y, o_z]^T \quad (19)$$

$$o_x = \frac{\sin(\alpha + \varphi_4)\sin \varphi_5}{\sqrt{2}} - \frac{\cos(\alpha + \varphi_4)(1 + \cos \varphi_5)}{2} \quad (20)$$

$$o_y = -\frac{\cos(\alpha + \varphi_4)\sin \varphi_5}{\sqrt{2}} - \frac{\sin(\alpha + \varphi_4)(1 + \cos \varphi_5)}{2} \quad (21)$$

$$o_z = \frac{(1 - \cos \varphi_5)}{2} \quad (22)$$

$$\vec{n} = [n_x, n_y, n_z]^T \quad (23)$$

$$n_x = -\sin(\alpha + \varphi_4)\cos \varphi_5 - \frac{\cos(\alpha + \varphi_4)\sin \varphi_5}{\sqrt{2}} \quad (24)$$

$$n_y = \cos(\alpha + \varphi_4)\cos \varphi_5 - \frac{\sin(\alpha + \varphi_4)\sin \varphi_5}{\sqrt{2}} \quad (25)$$

$$n_z = -\frac{\sin \varphi_5}{\sqrt{2}} \quad (26)$$

Closed-form inverse kinematics solutions

Usually, the inverse kinematics problems for a robot manipulator are to solve the joint positions given the positions and orientations of the end-effector relative to the base reference frame and the geometry parameters. The disadvantages of numerical solutions are that they are slower than closed-form solutions, and in some cases, they do not allow computation of all possible solutions.³² Thus, closed-form solutions are desirable because they are faster and readily determine all possible solutions.

The structure of this robot manipulator satisfies the Pieper criterion,³³ hence the algebraic method can be used to find the set of closed-form solutions. In this article, a newly appropriate set of closed-form solutions, which can avoid multiple solutions, is proposed to improve the already proposed set of closed-form solutions with the possibility of multiple solutions in our article.³⁰ The main differences are that the

proposed closed-form solutions in this article (using the results of forward kinematics p_x , p_y , p_z , a_x , a_y , a_z , and n_z) can lead to a unique solution for the inverse kinematics. Whereas the article³⁰ offers two solutions for φ_5 and likewise two solutions for φ_4 , X_1 (φ_1) and X_2 (φ_2) corresponding to these two solutions of φ_5 , and a unique solution X_3 (φ_3) (where the results of forward kinematics p_x , p_y , p_z , a_x , a_y , and a_z are used). The unique solution for the inverse kinematics is bound to be desirable and this is an important advantage of the proposed set of closed-form solutions, beyond its computational efficiency, because it does not only compute a single set of solutions but also could be programmed in an easy-to-use time-efficient closed form. The proposed set of closed-form solutions for the inverse kinematics is expressed as follows.

Solving φ_5 . Equations (18) and (26) can be rewritten as

$$\cos \varphi_5 = 2a_z - 1 \quad (27)$$

and

$$\sin \varphi_5 = -\sqrt{2}n_z \quad (28)$$

Based on equations (27) and (28), φ_5 is obtained as

$$\varphi_5 = \arctan 2(-\sqrt{2}n_z, 2a_z - 1) \quad (29)$$

Solving φ_4 . Let us define as

$$\theta = \alpha + \varphi_4 \quad (30)$$

Substituting equation (30) into equations (16) and (17) yields

$$\sin \theta = \frac{2a_y(\cos \varphi_5 - 1) - 2\sqrt{2}a_x \sin \varphi_5}{2 \sin^2 \varphi_5 + (1 - \cos \varphi_5)^2} \quad (31)$$

and

$$\cos \theta = \frac{2a_x(\cos \varphi_5 - 1) + 2\sqrt{2}a_y \sin \varphi_5}{2 \sin^2 \varphi_5 + (1 - \cos \varphi_5)^2} \quad (32)$$

Based on equations (31) and (32), giving

$$\begin{aligned} \theta &= \arctan 2(a_y(\cos \varphi_5 - 1) - \sqrt{2}a_x \sin \varphi_5, \\ &\quad a_x(\cos \varphi_5 - 1) + \sqrt{2}a_y \sin \varphi_5) \end{aligned} \quad (33)$$

Substituting equations (27) and (28) into equation (33) yields

$$\theta = \arctan 2(a_y(a_z - 1) + a_x n_z, a_x(a_z - 1) - a_y n_z) \quad (34)$$

According to equation (13), yielding

$$\sin \alpha = \frac{[p_y + e \sin(\alpha + \varphi_4) - L_p \sin(\alpha + \varphi_4)(\cos \varphi_5 - 1)/2 - L_p \cos(\alpha + \varphi_4) \sin \varphi_5/\sqrt{2}]}{L_3} \quad (35)$$

Substituting equations (27), (28), (30), (31), and (32) into equation (35) yields

$$\sin \alpha = \frac{[p_y - L_p a_y + e(a_y(a_z - 1) + a_x n_z)/((a_z - 1)^2 + n_z^2)]}{L_3} \quad (36)$$

Because the available range of the rotation angle is $\alpha \in (-\pi/4, \pi/4)$ as mentioned above, α can be obtained as

$$\alpha = \arctan 2(\sin \alpha, \sqrt{1 - \sin^2 \alpha}) \quad (37)$$

Substituting equation (36) into equation (37) yields

$$\alpha = \arctan 2(p_y - L_p a_y + e(a_y(a_z - 1) + a_x n_z)/((a_z - 1)^2 + n_z^2)) \\ \sqrt{1 - [p_y - L_p a_y + e(a_y(a_z - 1) + a_x n_z)/((a_z - 1)^2 + n_z^2)]^2}, \quad (38)$$

Substituting equations (34) and (38) into equation (30), φ_4 is given as

$$\varphi_4 = \theta - \alpha \quad (39)$$

Solving X_3 (φ_3). According to equations (14) and (27), X_3 and φ_3 are expressed as

$$X_3 = p_z - (L_2 + L_4 + \sqrt{2}L_5 + L_{01} + e + a_z L_p) \quad (40)$$

$$\varphi_3 = \frac{2\pi X_3}{s_z} \quad (41)$$

Solving X_1 (φ_1) and X_2 (φ_2). According to equation (1), giving

$$\tan \alpha = \frac{(X_2 - X_1)}{L_1} \quad (42)$$

Combining equations (12) and (42) leads to

$$\begin{cases} X_2 - X_1 = L_1 \tan \alpha \\ X_2 + X_1 = 2(p_x + e \cos(\alpha + \varphi_4) - L_3 \cos \alpha) \\ - L_p [\cos(\alpha + \varphi_4)(\cos \varphi_5 - 1) - \sqrt{2} \sin(\alpha + \varphi_4) \sin \varphi_5] \end{cases} \quad (43)$$

According to equation (43), X_1 (φ_1) and X_2 (φ_2) are expressed as

$$\begin{aligned} X_1 &= p_x + e \cos(\alpha + \varphi_4) \\ &- L_3 \cos \alpha - L_p [\cos(\alpha + \varphi_4)(\cos \varphi_5 - 1)/2 \\ &- \sin(\alpha + \varphi_4) \sin \varphi_5/\sqrt{2}] - (L_1 \tan \alpha)/2 \end{aligned} \quad (44)$$

$$\varphi_1 = \frac{2\pi X_1}{s_x} \quad (45)$$

and

$$\begin{aligned} X_2 &= p_x + e \cos(\alpha + \varphi_4) \\ &- L_3 \cos \alpha - L_p [\cos(\alpha + \varphi_4)(\cos \varphi_5 - 1)/2 \\ &- \sin(\alpha + \varphi_4) \sin \varphi_5/\sqrt{2}] + (L_1 \tan \alpha)/2 \end{aligned} \quad (46)$$

$$\varphi_2 = \frac{2\pi X_2}{s_x} \quad (47)$$

The results of X_1 (φ_1) and X_2 (φ_2) are obtained by substituting the group of α , φ_4 , and φ_5 into the above equations.

Dynamics of the robot manipulator

There are many tasks that require effective trajectory tracking capabilities. In order to improve the trajectory tracking performance, it should take account of the robot manipulator dynamic model via the model-based control strategies, such as the inverse dynamics control and the computed-torque-like technique. Also, the dynamic analysis can guide the design and construction of robotic systems and the selection of the actuators and transmission drive components to power the movement. Hence, dynamics is very critical to mechanical design, control, and simulation. The dynamic equations of motion can provide the relationships between the actuation and contact forces applied on robot mechanisms, and the consequent acceleration and motion trajectories. Because of the need for real-time implementation, especially in control, the robotics community has focused on the problem of computational efficiency. For inverse dynamics, the RNEA (which is an $O(n)$ algorithm, where n is the number of DOFs in the mechanism) proposed by Luh et al.³⁴ remains the most important algorithm.³² The RNEA uses a Newton–Euler formulation of the problem, and this formulation is especially amenable to the development of efficient recursive algorithms for dynamics computations.

In this section, the dynamics problem (i.e. inverse dynamics problem) of this 5-DOF robot manipulator is solved based on this very efficient RNEA. The velocity and acceleration of each link and the resultant forces on each link are first computed through an outward recursion in turn, starting with the known velocity and acceleration of the fixed base, and working toward the tips. A second, inward recursion uses the force balance equations at each link to compute the spatial force across

each joint and the value of each joint torque/force variable. Note that without loss of generality, only the case of the rigid robot manipulator is stressed here; other contributing factors in the dynamic description of the robot manipulator (which may include the dynamics of the actuators, joint and link flexibility, friction, noise, and disturbances) are not considered in this article.

Outward recursion

Link 1. As mentioned above, link 1 is driven in parallel by M_1 and M_2 , and a coupled movement relationship is generated. Here, the velocity and acceleration of link 1 relative to reference frame 1 are directly calculated according to these variables of link 1 relative to reference frame 0.

The velocity and acceleration of link 1 relative to reference frame 0 are given as follows

$${}^0\bar{\omega}_1 = [0, 0, \dot{\alpha}]^T \quad (48)$$

$${}^0\bar{v}_1 = {}^0\dot{P}_1 \quad (49)$$

$${}^0\dot{\omega}_1 = [0, 0, \ddot{\alpha}]^T \quad (50)$$

$${}^0\ddot{v}_1 = {}^0\dot{v}_0 + {}^0\ddot{P}_1 \quad (51)$$

where

$${}^0\dot{v}_0 = [0, 0, -g]^T = [0, 0, -9.80665]^T \quad (52)$$

$${}^0\dot{P}_1 = \left[\frac{s_x(\dot{\varphi}_1 + \dot{\varphi}_2)}{4\pi}, 0, 0 \right]^T \quad (53)$$

$${}^0\ddot{P}_1 = \left[\frac{s_x(\ddot{\varphi}_1 + \ddot{\varphi}_2)}{4\pi}, 0, 0 \right]^T \quad (54)$$

Let two new variables be defined as $k_1 = 2\pi L_1/s_x$ and $k_2 = k_1^2 + (\varphi_2 - \varphi_1)^2$, and according to equations (1)–(3), giving

$$\dot{\alpha} = \frac{k_1(\dot{\varphi}_2 - \dot{\varphi}_1)}{k_2} \quad (55)$$

$$\ddot{\alpha} = \frac{[k_1 k_2 (\ddot{\varphi}_2 - \ddot{\varphi}_1) - 2k_1(\dot{\varphi}_2 - \dot{\varphi}_1)^2(\varphi_2 - \varphi_1)]}{k_2^2} \quad (56)$$

The velocity and acceleration of link 1 relative to reference frame 1 and the inertia force and the moment acting on link 1 relative to center of mass of link 1 are derived as

$${}^1\bar{\omega}_1 = {}^1R_0 \cdot {}^0\bar{\omega}_1 \quad (57)$$

$${}^1\bar{v}_1 = {}^1R_0 \cdot {}^0\bar{v}_1 \quad (58)$$

$${}^1\dot{\omega}_1 = {}^1R_0 \cdot {}^0\dot{\omega}_1 \quad (59)$$

$${}^1\dot{v}_1 = {}^1R_0 \cdot {}^0\dot{v}_1 \quad (60)$$

$${}^1\dot{\bar{v}}_{c1} = {}^1\dot{v}_1 + {}^1\dot{\omega}_1 \times {}^1\bar{r}_{c1} + {}^1\bar{\omega}_1 \times ({}^1\bar{\omega}_1 \times {}^1\bar{r}_{c1}) \quad (61)$$

$${}^1\bar{f}_{c1} = m_1 \cdot {}^1\dot{v}_{c1} \quad (62)$$

$${}^1\bar{n}_{c1} = {}^{c1}I_1 \cdot {}^1\dot{\omega}_1 + {}^1\bar{\omega}_1 \times ({}^{c1}I_1 \cdot {}^1\bar{\omega}_1) \quad (63)$$

where

$${}^1R_0 = \begin{bmatrix} \cos \alpha & \sin \alpha & 0 \\ -\sin \alpha & \cos \alpha & 0 \\ 0 & 0 & 1 \end{bmatrix} \quad (64)$$

Link 2. The velocity and acceleration of link 2 relative to reference frame 2 and the inertia force and the moment acting on link 2 relative to center of mass of link 2 are obtained as

$${}^2\bar{\omega}_2 = {}^2R_1 \cdot {}^1\bar{\omega}_1 \quad (65)$$

$${}^2\dot{\bar{\omega}}_2 = {}^2R_1 \cdot {}^1\dot{v}_1 \quad (66)$$

$$\begin{aligned} {}^2\dot{v}_2 &= {}^2R_1 \cdot \left[{}^1\dot{v}_1 + {}^1\dot{\omega}_1 \times {}^1\bar{P}_2 + {}^1\bar{\omega}_1 \times ({}^1\bar{\omega}_1 \times {}^1\bar{P}_2) \right. \\ &\quad \left. + {}^2\bar{\omega}_2 \times {}^2\bar{z}_1 \cdot \dot{d}_2 + {}^2\bar{z}_1 \cdot \ddot{d}_2 \right] \end{aligned} \quad (67)$$

$${}^2\dot{v}_{c2} = {}^2\dot{v}_2 + {}^2\dot{\bar{\omega}}_2 \times {}^2\bar{r}_{c2} + {}^2\bar{\omega}_2 \times ({}^2\bar{\omega}_2 \times {}^2\bar{r}_{c2}) \quad (68)$$

$${}^2\bar{f}_{c2} = m_2 \cdot {}^2\dot{v}_{c2} \quad (69)$$

$${}^2\bar{n}_{c2} = {}^{c2}I_2 \cdot {}^2\dot{\bar{\omega}}_2 + {}^2\bar{\omega}_2 \times ({}^{c2}I_2 \cdot {}^2\bar{\omega}_2) \quad (70)$$

where

$${}^1\bar{P}_2 = \left[L_3, 0, \frac{s_z \varphi_3}{2\pi} + L_{01} \right]^T \quad (71)$$

$$\dot{d}_2 = \frac{s_z \dot{\varphi}_3}{2\pi} \quad (72)$$

$$\ddot{d}_2 = \frac{s_z \ddot{\varphi}_3}{2\pi} \quad (73)$$

$${}^2\bar{z}_1 = [0, 0, 1]^T \quad (74)$$

$${}^2R_1 = \begin{bmatrix} 1 & 0 & 0 \\ 0 & 1 & 0 \\ 0 & 0 & 1 \end{bmatrix} \quad (75)$$

Link 3. The velocity and acceleration of link 3 relative to reference frame 3 and the inertia force and the moment acting on link 3 relative to center of mass of link 3 are calculated as follows

$${}^3\bar{\omega}_3 = {}^3R_2 \cdot {}^2\bar{\omega}_2 + {}^3\bar{z}_2 \cdot \dot{\varphi}_4 \quad (76)$$

$${}^3\dot{\bar{\omega}}_3 = {}^3R_2 \cdot ({}^2\dot{\bar{\omega}}_2 + {}^2\bar{\omega}_2 \times {}^3\bar{z}_2 \cdot \dot{\varphi}_4) + {}^3\bar{z}_2 \cdot \ddot{\varphi}_4 \quad (77)$$

Table 3. The mass, center of mass, and moment of inertia of the robot manipulator.

Link	Mass (kg)	Moment of inertia (kg mm ²)	Center of mass (mm)
1	83.025	$\begin{bmatrix} 5095170.782 & -61.008 & 1019.065 \\ -61.008 & 3291706.841 & -15.858 \\ 1019.065 & -15.858 & 2367692.766 \end{bmatrix}$	$\begin{bmatrix} 0 \\ 0 \\ -44.182 \end{bmatrix}$
2	21.333	$\begin{bmatrix} 1475990.573 & -3970.014 & -748196.633 \\ -3970.014 & 2366543.574 & -8327.223 \\ -748196.633 & -8327.223 & 911968.216 \end{bmatrix}$	$\begin{bmatrix} -304.563 \\ -1.306 \\ -278.925 \end{bmatrix}$
3	8.022	$\begin{bmatrix} 142265.977 & -0.114 & 0.002 \\ -0.114 & 45016.139 & 46002.096 \\ 0.002 & 46002.096 & 109393.601 \end{bmatrix}$	$\begin{bmatrix} 0 \\ -63.686 \\ -468.138 \end{bmatrix}$
4	9.120	$\begin{bmatrix} 119573.680 & 27.342 & -0.849 \\ 27.342 & 36160.108 & -18452.465 \\ -0.849 & -18452.465 & 94076.578 \end{bmatrix}$	$\begin{bmatrix} 0 \\ -52.909 \\ -261.241 \end{bmatrix}$

$$\dot{\vec{v}}_3 = {}^3R_2 \cdot \left[\dot{\vec{v}}_2 + {}^2\vec{\omega}_2 \times {}^2\vec{P}_3 + {}^2\vec{\omega}_2 \times ({}^2\vec{\omega}_2 \times {}^2\vec{P}_3) \right] \quad (78)$$

$$\dot{\vec{v}}_{c3} = \dot{\vec{v}}_3 + {}^3\vec{\omega}_3 \times {}^3\vec{r}_{c3} + {}^3\vec{\omega}_3 \times ({}^3\vec{\omega}_3 \times {}^3\vec{r}_{c3}) \quad (79)$$

$$\dot{\vec{f}}_{c3} = m_3 \cdot \dot{\vec{v}}_{c3} \quad (80)$$

$$\vec{n}_{c3} = {}^cI_3 \cdot {}^3\vec{\omega}_3 + {}^3\vec{\omega}_3 \times ({}^cI_3 \cdot {}^3\vec{\omega}_3) \quad (81)$$

where

$$\vec{P}_3 = [0, 0, L_2 + L_4 + \sqrt{2}L_5]^T \quad (82)$$

$$\vec{z}_2 = \left[0, \frac{\sqrt{2}}{2}, \frac{\sqrt{2}}{2} \right]^T \quad (83)$$

$${}^3R_2 = \begin{bmatrix} \sin \varphi_4 & -\cos \varphi_4 & 0 \\ \cos \varphi_4 / \sqrt{2} & \sin \varphi_4 / \sqrt{2} & \sqrt{2}/2 \\ -\cos \varphi_4 / \sqrt{2} & -\sin \varphi_4 / \sqrt{2} & \sqrt{2}/2 \end{bmatrix} \quad (84)$$

Link 4. The velocity and acceleration of link 4 relative to reference frame 4 and the inertia force and the moment acting on link 4 relative to center of mass of link 4 are given as follows

$$\dot{\vec{\omega}}_4 = {}^4R_3 \cdot {}^3\vec{\omega}_3 + {}^4\vec{z}_3 \cdot \dot{\varphi}_5 \quad (85)$$

$$\ddot{\vec{\omega}}_4 = {}^4R_3 \cdot {}^3\dot{\vec{\omega}}_3 + {}^4R_3 \cdot {}^3\vec{\omega}_3 \times {}^4\vec{z}_3 \cdot \dot{\varphi}_5 + {}^4\vec{z}_3 \cdot \ddot{\varphi}_5 \quad (86)$$

$$\dot{\vec{v}}_4 = {}^4R_3 \cdot \left[\dot{\vec{v}}_3 + {}^3\vec{\omega}_3 \times {}^3\vec{P}_4 + {}^3\vec{\omega}_3 \times ({}^3\vec{\omega}_3 \times {}^3\vec{P}_4) \right] \quad (87)$$

$$\dot{\vec{v}}_{c4} = \dot{\vec{v}}_4 + {}^4\vec{\omega}_4 \times {}^4\vec{r}_{c4} + {}^4\vec{\omega}_4 \times ({}^4\vec{\omega}_4 \times {}^4\vec{r}_{c4}) \quad (88)$$

$$\dot{\vec{f}}_{c4} = m_4 \cdot \dot{\vec{v}}_{c4} \quad (89)$$

$$\vec{n}_{c4} = {}^cI_4 \cdot {}^4\vec{\omega}_4 + {}^4\vec{\omega}_4 \times ({}^cI_4 \cdot {}^4\vec{\omega}_4) \quad (90)$$

where

$${}^3\vec{P}_4 = [0, 0, \sqrt{2}e]^T \quad (91)$$

$${}^4\vec{z}_3 = \left[0, \frac{\sqrt{2}}{2}, \frac{\sqrt{2}}{2} \right]^T \quad (92)$$

$${}^4R_3 = \begin{bmatrix} -\cos \varphi_5 & -\sin \varphi_5 & 0 \\ \sin \varphi_5 / \sqrt{2} & -\cos \varphi_5 / \sqrt{2} & \sqrt{2}/2 \\ -\sin \varphi_5 / \sqrt{2} & \cos \varphi_5 / \sqrt{2} & \sqrt{2}/2 \end{bmatrix} \quad (93)$$

The mass (m_i), center of mass (${}^i\vec{r}_{ci}$), and moment of inertia about the center of mass (cI_i) of link i relative to reference frame i are listed in Table 3.

Inward recursion

Link 4. Suppose that the sums of all relevant external forces and moments applied on the operation point of the end-effector are \vec{f}_{tool} and \vec{n}_{tool} , respectively. Thus, the force and moment of link 4 applied on this operation point are ${}^5\vec{f}_5 = -\vec{f}_{tool}$ and ${}^5\vec{n}_5 = -\vec{n}_{tool}$, respectively. The force and moment of link 4 relative to the origin of coordinate frame 4 and the required joint actuator torque of the joint 5 are derived as

$${}^4\vec{f}_4 = {}^4R_5 \cdot {}^5\vec{f}_5 + {}^4\vec{f}_{c4} \quad (94)$$

$${}^4\vec{n}_4 = {}^4R_5 \cdot {}^5\vec{n}_5 + {}^4\vec{n}_{c4} + {}^4\vec{r}_{c4} \times {}^4\vec{f}_{c4} + {}^4\vec{P}_5 \times ({}^4R_5 \cdot {}^5\vec{f}_5) \quad (95)$$

$$\vec{\tau}_5 = {}^4\vec{z}_3^T \cdot {}^4\vec{n}_4 \quad (96)$$

where

$${}^4\vec{P}_5 = [0, 0, L_p]^T \quad (97)$$

$${}^4R_5 = \begin{bmatrix} 1 & 0 & 0 \\ 0 & 1 & 0 \\ 0 & 0 & 1 \end{bmatrix} \quad (98)$$

Link 3. The force and moment of link 3 relative to the origin of coordinate frame 3 and the required joint actuator torque of the joint 4 are obtained as

$${}^3\vec{f}_3 = {}^3R_4 \cdot {}^4\vec{f}_4 + {}^3\vec{f}_{c3} \quad (99)$$

$$\begin{aligned} {}^3\vec{n}_3 &= {}^4R_3^T \cdot {}^4\vec{n}_4 + {}^3\vec{n}_{c3} + {}^3\vec{r}_{c3} \\ &\times {}^3\vec{f}_{c3} + {}^3\vec{P}_4 \times ({}^4R_3^T \cdot {}^4\vec{f}_4) \end{aligned} \quad (100)$$

$$\vec{\tau}_4 = {}^3\vec{z}_2^T \cdot {}^3\vec{n}_3 \quad (101)$$

Link 2. The force and moment of link 2 relative to the origin of coordinate frame 2 and the required joint actuator force of the joint 3 are expressed as follows

$${}^2\vec{f}_2 = {}^2R_3 \cdot {}^3\vec{f}_3 + {}^2\vec{f}_{c2} \quad (102)$$

$$\begin{aligned} {}^2\vec{n}_2 &= {}^3R_2^T \cdot {}^3\vec{n}_3 + {}^2\vec{n}_{c2} + {}^2\vec{r}_{c2} \times {}^2\vec{f}_{c2} + {}^2\vec{P}_3 \times ({}^3R_2^T \cdot {}^3\vec{f}_3) \\ &\quad (103) \end{aligned}$$

$$\vec{F}_3 = {}^2\vec{z}_1^T \cdot {}^2\vec{f}_2 \quad (104)$$

Link 1. The force and moment of link 1 relative to the origin of coordinate frame 1 are given as follows

$${}^1\vec{f}_1 = {}^1R_2 \cdot {}^2\vec{f}_2 + {}^1\vec{f}_{c1} \quad (105)$$

$$\begin{aligned} {}^1\vec{n}_1 &= {}^1R_2 \cdot {}^2\vec{n}_2 + {}^1\vec{n}_{c1} + {}^1\vec{r}_{c1} \times {}^1\vec{f}_{c1} + {}^1\vec{P}_2 \times ({}^1R_2 \cdot {}^2\vec{f}_2) \\ &\quad (106) \end{aligned}$$

The interaction forces between link 1 and screw joints (consisting of ball screws) are shown in Figure 3. Combining Newton's and Euler's equations for link 1 leads to

$$\left\{ \begin{array}{l} \frac{{\vec{F}_2 - \vec{F}_1}}{\cos \alpha} \cdot \frac{L_1}{2 \cos \alpha} = {}^1\vec{z}_0^T \cdot ({}^0R_1 \cdot {}^1\vec{n}_1) \\ \vec{F}_2 + \vec{F}_1 = {}^1\vec{x}_0^T \cdot ({}^0R_1 \cdot {}^1\vec{f}_1) \end{array} \right. \quad (107)$$

where

$${}^1\vec{z}_0 = [0, 0, 1]^T \quad (108)$$

$${}^1\vec{x}_0 = [1, 0, 0]^T \quad (109)$$

The required joint actuator forces of joint 1 and joint 2 are derived by equation (107), that is

$$\vec{F}_1 = \frac{{}^1\vec{x}_0^T \cdot ({}^0R_1 \cdot {}^1\vec{f}_1)}{2} - \frac{{}^1\vec{z}_0^T \cdot ({}^0R_1 \cdot {}^1\vec{n}_1) \cdot \cos^2 \alpha}{L_1} \quad (110)$$

$$\vec{F}_2 = \frac{{}^1\vec{x}_0^T \cdot ({}^0R_1 \cdot {}^1\vec{f}_1)}{2} + \frac{{}^1\vec{z}_0^T \cdot ({}^0R_1 \cdot {}^1\vec{n}_1) \cdot \cos^2 \alpha}{L_1} \quad (111)$$

Control system of the robot manipulator

The performance and compliance of a robotic system are mainly ensured by a specially designed control system. In this section, the entire control system (which consists of the control system hardware and the control system software architecture) and the actual physical realization of the control system are presented.

Control system hardware

The control system hardware of this robot manipulator includes the following components: a control and servo drive unit, electricity supply circuitry unit, a terminal unit, and peripheral devices. A control schematic diagram (shown in Figure 4) is given to show the control structure and the communication between these components.

Control and servo drive unit. Thanks to the particular advantages of Ethernet for control automation

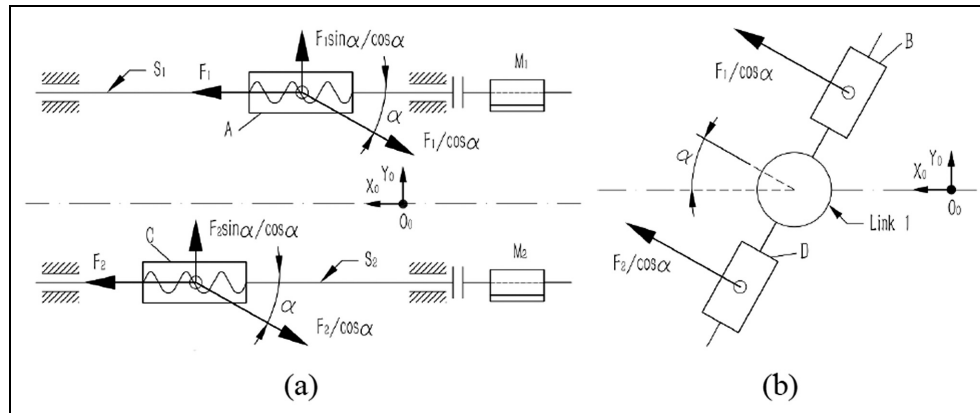


Figure 3. The interaction forces: (a) screw joints and (b) link 1.

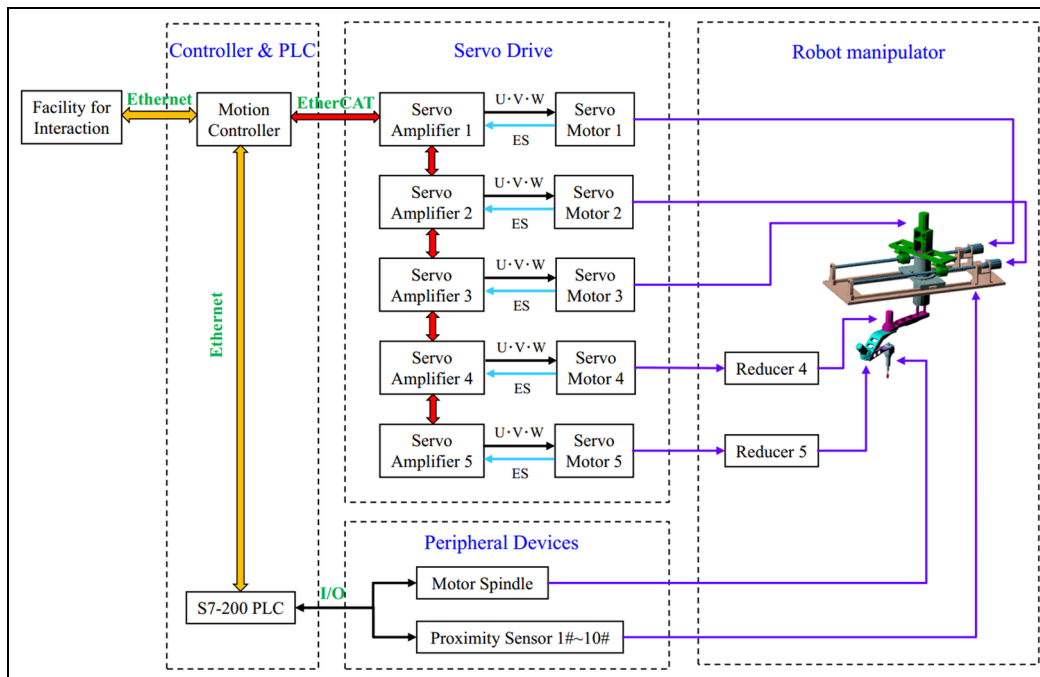


Figure 4. Control schematic diagram.



Figure 5. Motion controller: (a) GUC-ECAT motion controller and (b) teach pendant.

technology (EtherCAT),^{35,36} in this article, a motion controller, servo amplifiers, and servo motors, which can be compatible with EtherCAT technology, are selected to give a solution for the high-speed command transmission requirements of the control and servo drive unit.

In this article, a GUC-ECAT controller (model No. GUC-ECAT8-M23-L2-F4G) with a matching teach pendant, which is compatible with EtherCAT technology, is chosen as the motion controller for this robot manipulator (shown in Figure 5). This motion controller, which is manufactured by Googol Technology Ltd, can synchronously control up to eight axes. The main features include the following: (a) shortest sampling cycle and control cycle can reach 125 and 250 μ s, respectively; (b) development platform OtoStudio fully supports IEC61131-3 programming standard; (c) human machine interaction supports eHMI interface;

and (d) it supports remote diagnosis and analysis via Ethernet.

Both the first three axes J_1 , J_2 , and J_3 , and the last two axes J_4 and J_5 of this robot manipulator are actuated using alternating-current (AC) rotary servo motors (models no. are R2AA08075FCP29W and R2AA06020FCP29W, respectively) and the compatible EtherCAT interface type of servo amplifiers (models no. are RS2A03A0KA4 and RS2A01A0KA4, respectively). These servo motors and servo amplifiers are manufactured by Sanyo Electric Co., Ltd. The communication cycle of this new product (i.e. the servo amplifiers R advanced model EtherCAT Interface type) is short (125 μ s), and the position commands are subdivided, making device operations smoother and improving stabilizability and controllability.

The messages between the motion controller and servo amplifiers are communicated via EtherCAT

protocol, and the servo amplifier and its related optical battery-backup method absolute encoder of servo motor are communicated with serial data signal.

Electricity supply circuitry unit. Electrical power supply (appropriate voltages and currents for servo motor, servo amplifier, peripheral devices, etc.) is an important element of a robot manipulator control system. Hence, the related electricity supply circuitry arrangements should be designed for the application of electrical engineering. The application-specific transmitter circuitry contains the main circuit power supply, electric circuits of the servo amplifiers, and the appropriate switching circuits.

The main circuit power supply provides the power for the whole control system, which includes servo motor power supply, servo amplifier power supply, controller and programmable logic controller (PLC) power supply, motor spindle power supply, and trigger signal power supply. The high stabilizability and realizability of electric circuits for servo amplifiers have a great influence on the electric characteristics of servo amplifiers and servo motors. Through appropriate switching circuits (i.e. the circuits for the power supply of the servo amplifiers and servo motors, alarm circuits of the servo amplifiers, and operating status display circuits of the control system), some particular regions of the control system can be isolated at particular intersections.

Terminal unit. The main task of a terminal unit is to ensure interaction between the administrator/operator and the control system through information input/output (I/O) tools. Information exchange and some functions (such as activation/deactivation, running and executing user programs, robot manipulator status signaling, and interaction between the administrator/operator and the terminal unit software) can be implemented at the administrator/operator's console.

Since system control tasks are carried out in the motion controller, a specialized operating system for real-time task fulfillment is not required in the terminal unit. Advanced PLC capabilities (such as fast I/O control and synchronizing actions) can implement the coordinate operation of the peripheral devices and the control system. In this article, a PC for interaction which is equipped with a keyboard and a screen (with Windows 7, Intel(R) Core(TM) CPU i5-4570 at 3.20 GHz, 8.00 GB of RAM) and an advanced SIMATIC S7-200 PLC of Siemens AG with external I/O modules are selected as the terminal unit of the control system. The communication between the motion controller and PLC is achieved through the

predefined digital input (DI)/digital output (DO) of the motion controller and PLC, respectively.

Peripheral devices. The high-speed motor spindle (type: YD4040, produced by Wuxi Sunshine Precision Machinery Co., Ltd), with which the end-effector is equipped, and 10 inductive proximity sensors (which are manufactured by Omron Corporation and the type is E2E-X14MD1-Z) attached to the robot manipulator are the main peripheral devices of this robot manipulator. The peripheral devices (i.e. the motor spindle and inductive proximity sensors) and PLC are communicated with the corresponding predefined DI/DO.

Control system software

The control system software architecture of this robot manipulator consists of two main parts: motion controller software and PLC software. Since this robot manipulator is a new 5-DOF hybrid configuration, the forward and inverse kinematics for motion trajectory calculation must be programmed in the motion controller software according to the forward kinematics modeling and the proposed method for closed-form inverse kinematics solutions. This application is implemented on the CPAC software platform of the GUC-ECAT motion controller. Each axis of this motion controller can operate independently under five modes, point-to-point motion mode, jog motion mode, position-time (PT) motion mode, electronic gear motion mode, and follow motion mode. This motion controller software provides an EtherCAT library for the communication between EtherCAT slave devices and motion controller. This motion controller software also offers a programming environment, that is, the OtoStudio environment; the system configuration requirements for the status and the operation mode and the motion program written in the described language that will be transferred to the control unit (which is transformed into the internal representation) can be done under this programming environment. Additionally, the motion controller software can achieve hardware resource access (such as DI/DO, encoder, and discretionary access control), safety mechanism (such as soft limit, drive alarm, smooth stop and emergency stop, and error position limit), motion status detection, remote debug in VC++ or Visual Studio development environment, and so on.

The other main part of the control system software architecture, the PLC software, provides logic control and communication, sequence of operations, and multiple arrangements of DI/DO and analog I/O in the control system, the motion controller, and the peripheral devices (i.e. the motor spindle and inductive proximity sensors).

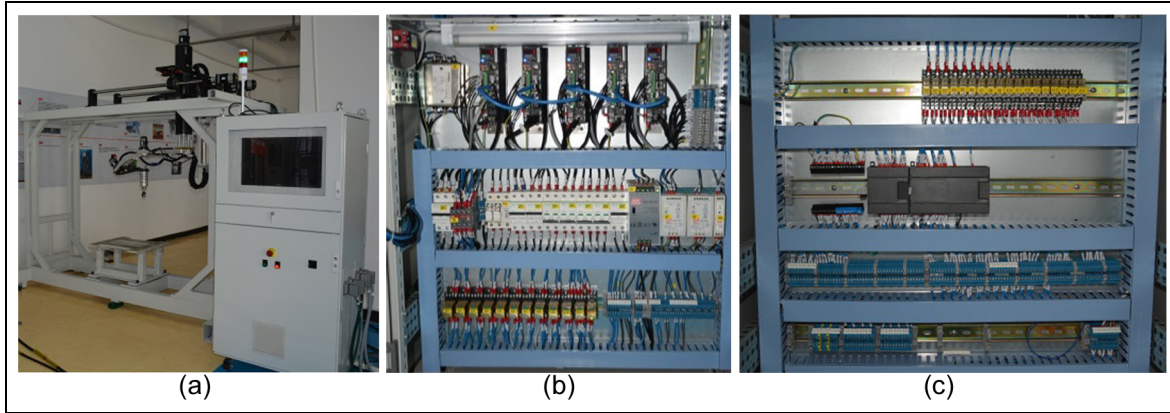


Figure 6. Control cabinet of the designed control system.

The actual physical implementation of the designed control system

The physical implementation of the corresponding circuitry and the entire control system are installed in a control cabinet, as shown in Figure 6.

Numerical examples and experiments

In this section, a kinematics simulation example and a dynamics simulation example based on the MATLAB and ADAMS are presented to verify the proposed set of closed-form solutions for the inverse kinematics and the derived dynamic equations for inverse dynamics, respectively. Additionally, two experiments are conducted on the physical prototype to test the repeatability and accuracy of both the position and path.

Kinematics numerical example

Just like our other article,³⁰ the same saddle surface is chosen for the kinematics simulation of this robot manipulator and for the simulation results' comparison between the proposed set of closed-form solutions in this article and the already proposed set of closed-form solutions in the article.³⁰

The equation of this saddle surface is given as

$$z = \frac{y^2}{200} - \frac{(x - 825)^2}{200} + 700 \quad (112)$$

The function of the end-effector trajectory is expressed as

$$\begin{cases} x = 700 + 5\eta(\text{mm}) \\ y = -125 + 5\eta(\text{mm}) \\ z = y^2/200 - (x - 825)^2/200 + 700(\text{mm}) \end{cases} \quad (113)$$

$$\eta \in [0, 50]$$

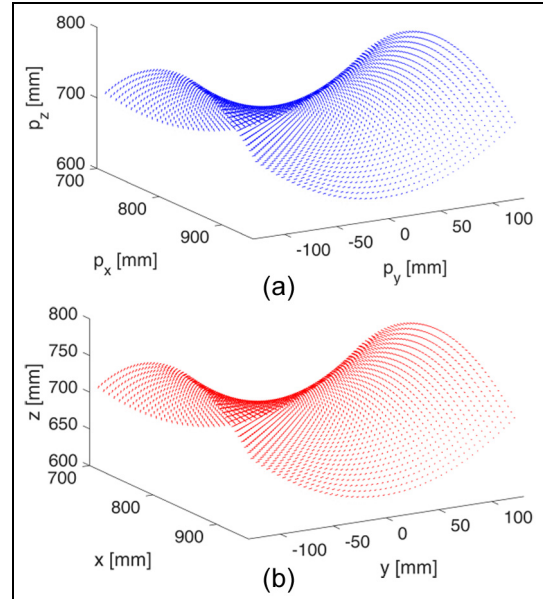


Figure 7. Saddle surface trajectory: (a) desired trajectory and (b) traversal trajectory.

MATLAB numerical simulation. The discrete positions $(p_x, p_y, p_z)^T$ of the desired trajectory are obtained by the given end-effector trajectory function (equation (113)). The motor spindle always points at each discrete position (i.e. each discrete orientation $(a_x, a_y, a_z)^T$ always equals the unit normal vector of the corresponding discrete position). The desired saddle trajectory is shown in Figure 7(a).

The joint angles $\varphi_1, \varphi_2, \varphi_3, \varphi_4$, and φ_5 are obtained according to the proposed set of closed-form solutions in this article. Using these obtained joint angles, the position $(x, y, z)^T$ and the motor spindle's orientation $(u, v, w)^T$ of the traversal trajectory are obtained by solving the forward kinematics as shown in Figure 7(b).

The position and the orientation of the motor spindle corresponding to the desired trajectory and the

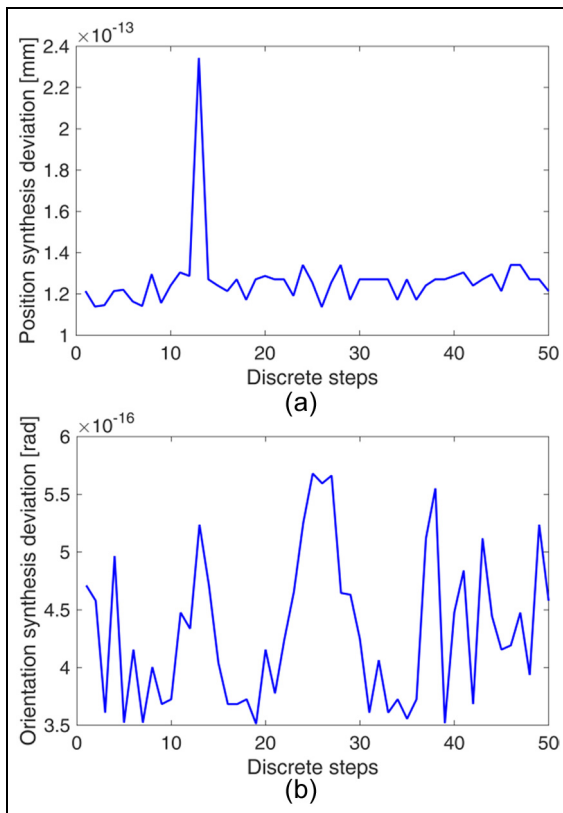


Figure 8. Synthesis deviation: (a) position synthesis deviation and (b) orientation synthesis deviation.

traversed trajectory are obtained through this MATLAB numerical simulation, respectively. The position and orientation synthesis deviation, Δd and $\Delta\delta$, are, respectively, defined as

$$\Delta d = \sqrt{(p_x - x)^2 + (p_y - y)^2 + (p_z - z)^2} \quad (114)$$

$$\Delta\delta = \sqrt{(a_x - u)^2 + (a_y - v)^2 + (a_z - w)^2} \quad (115)$$

The calculated synthesis deviations are shown in Figure 8, and the corresponding maximum values are obtained as

$$\Delta d_{\max} = 2.3229 \times 10^{-13} \text{ mm} \quad (116)$$

$$\Delta\delta_{\max} = 5.6795 \times 10^{-16} \text{ rad} \quad (117)$$

Comparing the desired trajectory (which is obtained based on the given end-effector trajectory function) and the traversal trajectory (which is obtained by the discrete desired trajectory and the proposed set of closed-form solutions), the position and orientation synthesis deviations are all especially small. On the other hand, making a comparison between the maximum position and orientation synthesis deviations in this article (given by equations (116) and (117),

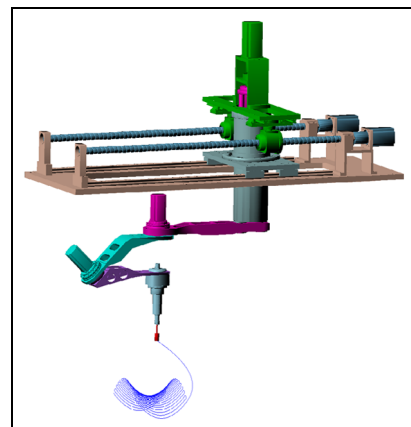


Figure 9. The simulation of the virtual prototype model.

respectively) and the ones in article by Guo et al.³⁰ (which are 2.3437×10^{-13} mm and 5.8915×10^{-16} rad, respectively), it can be found that these deviations are slightly different. These deviations are caused by the computational accuracy of the MATLAB software; therefore, the position and orientation synthesis deviation can both be considered to be 0. Hence, the newly proposed set of closed-form solutions for the inverse kinematics is valid and effective.

Virtual prototype simulation. In order to further validate the newly proposed set of closed-form solutions and observe the movement of this robot manipulator, a virtual prototype kinematics co-simulation is conducted in ADAMS and MATLAB. The virtual prototype model is generated in the ADAMS. The motion joint functions are obtained based on the joint angles (φ_1 , φ_2 , φ_3 , φ_4 , and φ_5) using the proposed set of closed-form solutions in a MATLAB simulation for inverse kinematics of this robot manipulator. The simulation result and the virtual prototype model are shown in Figure 9. The movements of the end-effector and other movable components are dexterous and smooth.

Comparing the traversed saddle trajectory in ADAMS and the desired saddle trajectory in MATLAB, a desirable match can be found (the magnitude of the synthesis deviations is within 10^{-10}). That also validates the correctness of the calculation of the end-effector's orientations, which are determined by the normal vector at each discrete position on the desired surface. Thus, the feasibility and validity of the newly proposed set of closed-form solutions for the inverse kinematics are verified.

Dynamics simulation

An example of the inverse dynamics problem of this robot manipulator is solved using the numerical

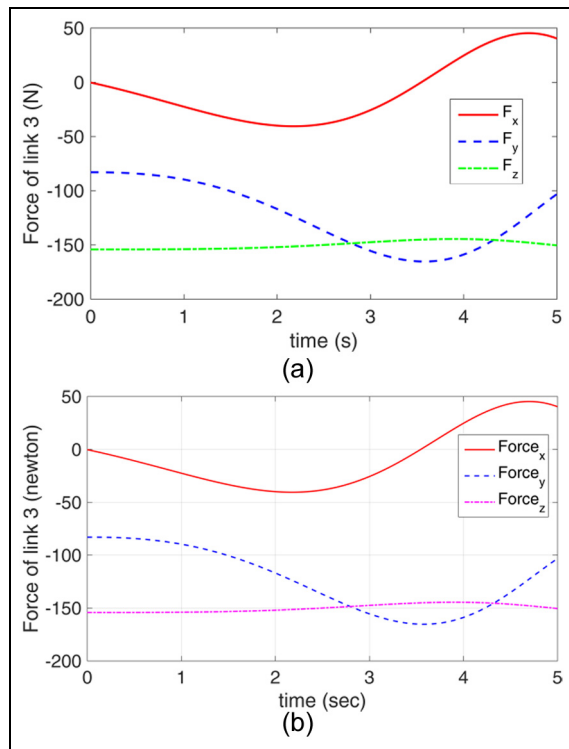


Figure 10. The force of link 3: (a) simulation in MATLAB and (b) simulation in ADAMS.

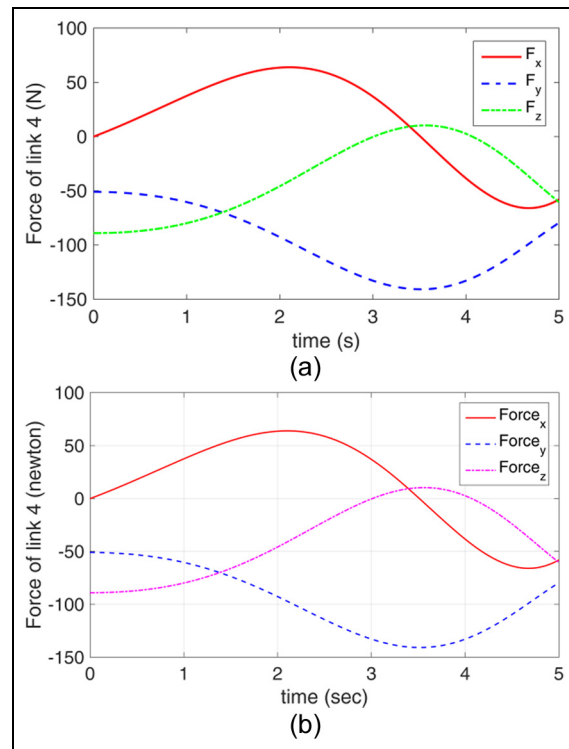


Figure 12. The force of link 4: (a) simulation in MATLAB and (b) simulation in ADAMS.

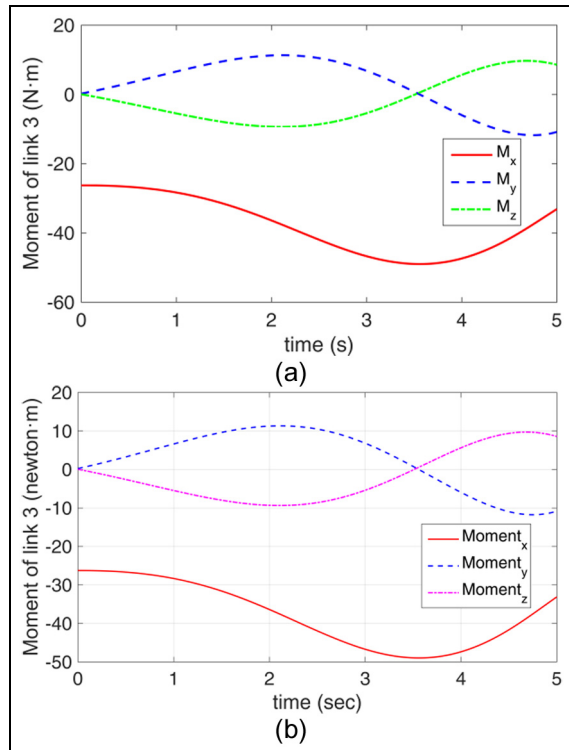


Figure 11. The moment of link 3: (a) simulation in MATLAB and (b) simulation in ADAMS.

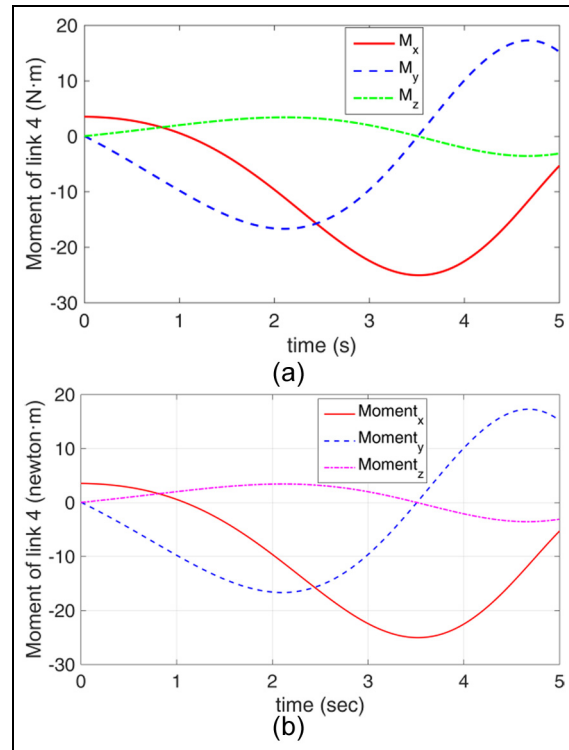


Figure 13. The moment of link 4: (a) simulation in MATLAB and (b) simulation in ADAMS.

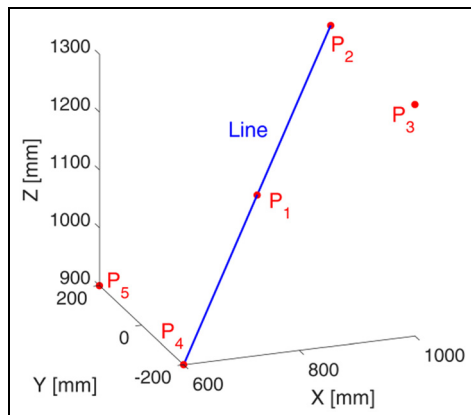


Figure 14. The preprogrammed five locations and straight line path.

programs of the derived dynamic equations (in MATLAB) and the virtual prototype model (in ADAMS/View), respectively. The conditions under which the inverse dynamics computations of this robot manipulator are performed for this example are given as follows: the sums of all relevant external forces (acting on the operation point of the end-effector, that is, the reference frame origin O_3) is $\bar{f}_{tool} = 50$ N; the functions of each joint angle are $\varphi_1 = 3\pi(t^2 + 11t)/4$ rad, $\varphi_2 = \pi(t^2 + 11t)$ rad, $\varphi_3 = \pi(t^2 + 7t)/2$ rad, $\varphi_4 = \pi(t^2 + 5t)/30$ rad, and $\varphi_5 = \pi(t^2 + 5t)/30$ rad; the total simulation time is 5 s.

Here, the forces and moments of links 3 and 4 (relative to the reference frame origin O_3 and O_4 , respectively) are given as an example, considering that the results of dynamics computations of the derived dynamic equations may or may not be equal to the results of the virtual prototype simulation. The forces and moments of links 3 and 4 computed by numerical programs in MATLAB are shown in Figures 10(a), 11(a), 12(a), and 13(a), respectively. Additionally, the

forces and moments of links 3 and 4 are obtained by the simulation of the virtual prototype in ADAMS as shown in Figures 10(b), 11(b), 12(b), and 13(b), respectively. Comparing the forces and moments of links 3 and 4, the simulation results in MATLAB and ADAMS are consistent. Hence, the derived dynamic equations based on the RNEA are correct and valid.

Physical experiments

Industrial robot performance is often measured in functional operations by the repeatability and accuracy of the position and path. The position and path repeatability (i.e. the tolerance of the position and path at repeated program execution, respectively) represent the ability of the manipulator to repeatedly return to the same location or track the same trajectory, respectively. The position and path accuracy (i.e. the maximum deviation of the average of actual position and actual path at program execution from the programmed position and the programmed path, respectively) cover the ability of a robot manipulator to return to a preprogrammed location or follow along a preprogrammed path in space.

In this article, the test of the repeatability and accuracy for five preprogrammed locations and a preprogrammed straight line path (shown in Figure 14) are conducted on the physical prototype. The experiment physical prototype and the measuring equipment (i.e. a laser tracker and its type is Leica AT901-MR) are shown in Figure 15. In these experiments, the rated velocity is 200 mm/s; the rated numbers of test motion cycles of the preprogrammed locations and straight line path tests are 30 and 10, respectively. The locus of these preprogrammed locations and the trajectory of this preprogrammed straight line path are shown in Figures 16 and 17, respectively. The observed position repeatability,

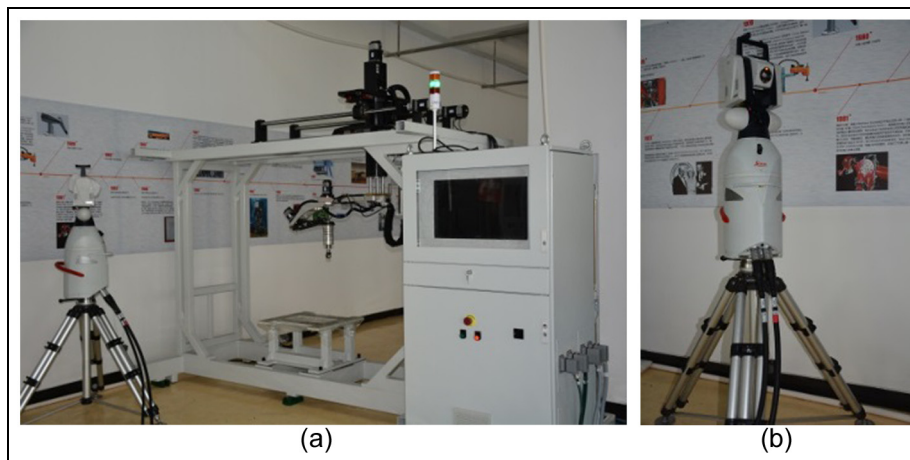


Figure 15. Experiment physical prototype and measuring equipment: (a) the physical prototype and (b) the laser tracker.

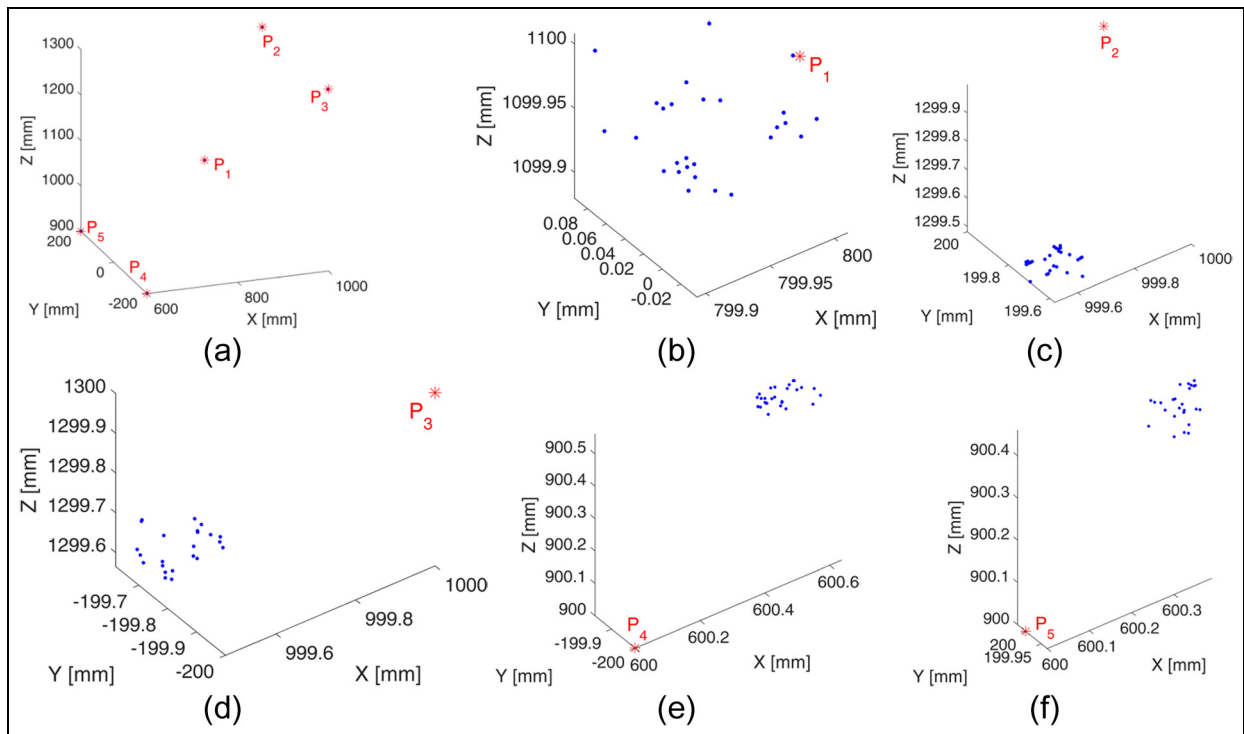


Figure 16. Total locus of the programmed locations: (a) all locations, (b) P₁, (c) P₂, (d) P₃, (e) P₄, and (f) P₅.

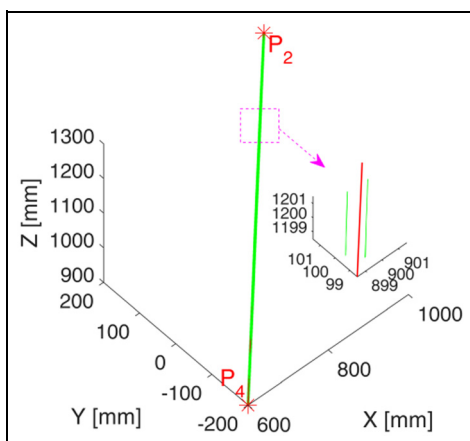


Figure 17. Trajectory of the programmed path.

position accuracy, path repeatability, and path accuracy are 0.063, 0.437, 0.021, and 0.612 mm, respectively.

Conclusion

The physical prototype of a new 5-DOF hybrid robot manipulator is developed. The mechanical structure, kinematics, dynamics, and the specially designed control system of this robot manipulator are presented.

The major contributions of this article can be summarized as follows:

1. The physical prototype and the specially designed control system of a new 5-DOF hybrid robot manipulator are developed, and the tests for the repeatability and accuracy are conducted on this physical prototype.
2. A newly appropriate set of closed-form solutions, which can avoid multiple solutions, is proposed to improve the already proposed method described in our other article and address the inverse kinematics problem for this robot manipulator and other similar structures.
3. The tests for the repeatability and accuracy of both the position and path and the validation of the kinematic equations and the dynamics equations of this robot manipulator are conducted in two experiments on the physical prototype and two software simulations, respectively.

In future work, the practical applications of this robot manipulator in processing of complex surfaces will be concerned. Furthermore, this robot manipulator will be integrated with a vision system to study work-piece reconstruction strategies.

Declaration of conflicting interests

The author(s) declared no potential conflicts of interest with respect to the research, authorship, and/or publication of this article.

Funding

The author(s) disclosed receipt of the following financial support for the research, authorship, and/or publication of this article: This work was supported by Self-Planned Task (no. SKLRS201609B) of State Key Laboratory of Robotics and System (HIT).

References

1. Gao Z and Zhang D. Performance analysis, mapping, and multiobjective optimization of a hybrid robotic machine tool. *IEEE T Ind Electron* 2015; 62: 423–433.
2. Bindal V, Gonzalez-Heredia R, Masrur M, et al. Technique evolution, learning curve, and outcomes of 200 robot-assisted gastric bypass procedures: a 5-year experience. *Obes Surg* 2015; 25: 997–1002.
3. Pisla D, Szilaghyi A, Vaida C, et al. Kinematics and workspace modeling of a new hybrid robot used in minimally invasive surgery. *Robot Cim: Int Manuf* 2013; 29: 463–474.
4. Zheng C, Liu J, Grift TE, et al. Design and analysis of a wheel-legged hybrid locomotion mechanism. *Adv Mech Eng* 2015; 7: 1–10.
5. Chai X, Fan J, Zhou L, et al. Study on telescope gain affected by a multilevel hybrid mechanism in FAST. *Adv Mech Eng* 2014; 6: 841526.
6. Xie F, Liu X-J and Wang C. Design of a novel 3-DoF parallel kinematic mechanism: type synthesis and kinematic optimization. *Robotica* 2015; 33: 622–637.
7. Xie F, Liu X-J, You Z, et al. Type synthesis of 2T1R-type parallel kinematic mechanisms and the application in manufacturing. *Robot Cim: Int Manuf* 2014; 30: 1–10.
8. Xie F, Liu X-J and Li T. Type synthesis and typical application of 1T2R-type parallel robotic mechanisms. *Math Probl Eng* 2013; 2013: 206181.
9. Yuan-Ming C, Wei-Xiang P and An-Chun H. Concentric hole drilling in multiple planes for experimental investigation of five-axis reconfigurable precision hybrid machine. *Int J Adv Manuf Tech* 2015; 76: 1253–1262.
10. Sangveraphunsiri V and Chooprasird K. Dynamics and control of a 5-DOF manipulator based on an H-4 parallel mechanism. *Int J Adv Manuf Tech* 2010; 52: 343–364.
11. Altuzarra O, Martín YS, Amezua E, et al. Motion pattern analysis of parallel kinematic machines: a case study. *Robot Cim: Int Manuf* 2009; 25: 432–440.
12. Wang L, Wu J, Li T, et al. A study on the dynamic characteristics of the 2-DOF redundant parallel manipulator of a hybrid machine tool. *Int J Robot Autom* 2015; 30: 184–191.
13. Wang L, Wu J, Wang J, et al. An experimental study of a redundantly actuated parallel manipulator for a 5-DOF hybrid machine tool. *IEEE/ASME T Mech* 2009; 14: 72–81.
14. Wu J, Wang J, Wang L, et al. Study on the stiffness of a 5-DOF hybrid machine tool with actuation redundancy. *Mech Mach Theory* 2009; 44: 289–305.
15. Wu J, Wang J, Wang L, et al. Dynamic model and force control of the redundantly actuated parallel manipulator of a 5-DOF hybrid machine tool. *Robotica* 2008; 27: 59–65.
16. Jiang S, Guo J, Liu S, et al. Kinematic analysis of a 5-DOF hybrid-driven MR compatible robot for minimally invasive prostatic interventions. *Robotica* 2012; 30: 1147–1156.
17. Gherman B, Pisla D, Vaida C, et al. Development of inverse dynamic model for a surgical hybrid parallel robot with equivalent lumped masses. *Robot Cim: Int Manuf* 2012; 28: 402–415.
18. Li Q, Wu W, Li H, et al. A hybrid robot for friction stir welding. *Proc IMechE, Part C: J Mechanical Engineering Science* 2015; 229: 2639–2650.
19. Zoppi M, Zlatanov D and Molino R. Kinematics analysis of the Exechon tripod. In: *Proceedings of the ASME 2010 international design engineering technical conferences and computers and information in engineering conference*, Montreal, QC, Canada, 15–18 August 2010, pp.1381–1388. New York: American Society of Mechanical Engineers.
20. Liu H, Huang T, Mei J, et al. Kinematic design of a 5-DOF hybrid robot with large workspace/limb-stroke ratio. *J Mech Des: T ASME* 2007; 129: 530–537.
21. Huang T, Li M, Zhao X, et al. Conceptual design and dimensional synthesis for a 3-DOF module of the TriVariant-a novel 5-DOF reconfigurable hybrid robot. *IEEE T Robot* 2005; 21: 449–456.
22. Hu B. Formulation of unified Jacobian for serial-parallel manipulators. *Robot Cim: Int Manuf* 2014; 30: 460–467.
23. Staffetti E. Kinesthetic analysis of robot manipulators using the Grassmann–Cayley algebra. *IEEE T Robotic Autom* 2004; 20: 200–210.
24. Tanev TK. Kinematics of a hybrid (parallel–serial) robot manipulator. *Mech Mach Theory* 2000; 35: 1183–1196.
25. Pott PP, Wagner A, Badreddin E, et al. Inverse dynamic model and a control application of a novel 6-DOF hybrid kinematics manipulator. *J Intell Robot Syst* 2011; 63: 3–23.
26. Tanner HG and Kyriakopoulos KJ. Mobile manipulator modeling with Kane's approach. *Robotica* 2001; 19: 675–690.
27. Krasilnikyants E, Varkov A and Tyutikov V. Robot manipulator control system. *Automat Rem Contr +* 2013; 74: 1589–1598.
28. Wai R-J and Muthusamy R. Fuzzy-neural-network inherited sliding-mode control for robot manipulator including actuator dynamics. *IEEE T Neural Netw Learn Syst* 2013; 24: 274–287.
29. You W, Kong M, Sun L, et al. Control system design for heavy duty industrial robot. *Ind Robot* 2012; 39: 365–380.
30. Guo W, Li R, Cao C, et al. Kinematics analysis of a novel 5-DOF hybrid manipulator. *Int J Autom Tech* 2015; 9: 765–774.

31. Denavit J. A kinematic notation for lower-pair mechanisms based on matrices. *J Appl Mech: T ASME* 1955; 22: 215–221.
32. Siciliano B and Khatib O. *Springer handbook of robotics*. Berlin: Springer, 2008.
33. Peiper DL. *The kinematics of manipulators under computer control*. PhD Thesis, Department of Computer Science, Stanford University, Stanford, CA, 1968.
34. Luh JY, Walker MW and Paul RP. On-line computational scheme for mechanical manipulators. *J Dyn Syst: T ASME* 1980; 102: 69–76.
35. Cena G, Bertolotti IC, Scanzio S, et al. Evaluation of EtherCAT distributed clock performance. *IEEE T Ind Inform* 2012; 8: 20–29.
36. Jansen D and Buttner H. Real-time Ethernet: the EtherCAT solution. *Comput Control Eng* 2004; 15: 16–21.